LETTER **Communicated by Idan Segev**

Understanding Parkinsonian Handwriting Through a Computational Model of Basal Ganglia

Garipelli Gangadhar
Gangadhar.Garipelli@idiap.ch
Machine Learning Group, IDIAP Research Institute, CH-1920 Martigny, Switzerland

Denny Joseph
denny_cns@yahoo.com
V. Srinivasa Chakravarthy
schakra@ee.iitm.ac.in
Department of Biotechnology, Indian Institute of Technology–Madras, Chennai, India 600036

Handwriting in Parkinson's disease (PD) is typically characterized by micrographia, jagged line contour, and unusual fluctuations in pen tip velocity. Although PD handwriting features have been used for diagnostics, they are not based on a signaling model of basal ganglia (BG). In this letter, we present a computational model of handwriting generation that highlights the role of BG. When PD conditions like reduced dopamine and altered dynamics of the subthalamic nucleus and globus pallidus externa subsystems are simulated, the handwriting produced by the model manifested characteristic PD handwriting distortions like micrographia and velocity fluctuations. Our approach to PD modeling is in tune with the perspective that PD is a dynamic disease.

1 Introduction

Handwriting is a learned, highly practiced human motor skill that involves control and coordination of complex movement sequences. Over the past decade, handwriting has been gaining attention as a source of diagnostic information (Cobbah & Fairhurst, 2000; Kuenstler, Juhnhold, Knapp, & Gertz, 1999; van Gemmert, Teulings, Contreras-Vidal, & Stelmach, 1999) and a window onto a variety of neurological disorders, including Parkinson's disease (PD) (van Gemmert et al., 1999; Teulings, Vidal, Stelmach, & Adler, 2002), schizophrenia (Gallucci, Phillips, Bradshaw, Vaddadi, & Pantelis, 1997), obsessive-compulsive disorder (OCD) (Mavrogiorgou et al., 2001), and Huntington's disease (Phillips, Bradshaw, Chiu, & Bradshaw, 1994). Since handwriting, unlike reaching or walking, is a high-level motor activity, it engages large parts of cortical and subcortical regions that include supplementary motor area (SMA), premotor area (PM), primary

(a) (b)

Figure 1: Handwriting samples (the word written is *SriRamajayam* in the Tamil language). (a) Normal handwriting (word written once). (b) Handwriting (word written three times) of a PD patient (52 years old).

motor area (M1), basal ganglia (BG), cerebellum, and spinal cord. Since each of these regions contributes to handwriting output in its own unique fashion, pathology of any of these regions is manifested as characteristic features of handwriting. Thus, handwriting movements are particularly suitable for analysis of motor impairments.

For example, in PD, a neurodegenerative disorder associated with pathology of BG, handwriting is marked by diminutive letter size, or micrographia (see Figure 1b), jagged handwriting contour and abnormal fluctuations in velocity and acceleration profile (van Gemmert et al., 1999; Teulings & Stelmach, 1991). Other PD symptoms include tremor, rigidity, bradykinesia, and postural abnormalities. The principal etiology of PD is the loss of dopaminergic neurons in the substantia nigra pars compacta (SNc), a nucleus in BG.

Handwriting features like stroke size, peak acceleration, stroke duration, ratio between mean, and standard deviation of stroke length or duration have been used for diagnosis of PD (Teulings & Stelmach, 1991; van Gemmert, Adler, & Stelmach, 2003; Phillips, Stelmach, & Teasdale, 1991). However, most such attempts treat the motor system as a "black box" and are based on empirical relationships between the handwriting parameters and the stage of maturity of the disease. Insight into the understanding of BG function and the precise role of these nuclei in handwriting generation is indispensable for producing an accurate computational model.

In this work, we present a computational model of BG and motor system that can generate handwriting that under pathological conditions, can exhibit typical symptoms of PD handwriting. We next discuss computational models available in the literature on PD, handwriting generation, and PD handwriting.

1.1 Computational Models of Handwriting Generation. One of the earliest ideas of handwriting models was to resolve handwritten stroke data into oscillatory components (Hollerbach, 1981; Schomaker, 1991; Kalveram, 1996). Hollerbach (1981) proposed that actual handwriting segments can be approximated by natural oscillations of an inertial load suspended

by two orthogonal pairs of opposing springs. Several authors attempted to fit such families of solutions to handwritten strokes or components (Plamondon, 1989; Schomaker, 1991). Schomaker proposed an oscillatory neural network model trained by a variation of the delta rule; however, training led to uncertain results. More recently Kalveram (1996) proposed a model in which stroke data are resolved to their Fourier components. For an oscillatory neural model of handwriting to be biologically viable, it has to address certain fundamental issues. The first key issue, preparing the initial state of the oscillatory network, does not seem to have received adequate attention in these models (Schomaker, 1991; Kalveram, 1996). Essentially there is a need for auxiliary mechanisms that (1) initiate and prepare (a rhythm in the oscillatory network's state), (2) align (that rhythm with respect to the time of onset of the stroke), and (3) terminate (the rhythm at the appropriate time). In Gangadhar, Joseph, and Chakravarthy (2007), we presented a model of handwriting generation that addresses these issues. In this letter, we combine the handwriting model (Gangadhar et al., 2007) with a model of the BG in order to study aspects of PD handwriting.

1.2 Models of Parkinson's Disease. Borrett, Yeap, and Kwan (1993) studied the dynamics of a four-layer neural network that simulates the type of computation made by dysfunctional cortico-BG-thalamic-cortical loop in PD. The model exhibits a variety of dynamic behaviors. Under dopamine-deficient conditions, the output of the network changes from a fixed-point attractor state to a periodic, tremulous state resembling Parkinsonian tremor. Edwards, Beuter, and Glass (1999) presented a network model of Parkinsonian tremor that can exhibit transition from irregular tremor to regular oscillations. A preliminary model of BG-related movement disorders was proposed by Mitchel, Brotchie, and Crossman (1991). A dynamic model of Parkinsonian reaching movements with (ON) and without (OFF) L-dopa medication was presented in Suri, Albani, and Glattfelder (1997).

1.3 Modeling PD Handwriting. van Gemmert et al. (1999) made computer simulations of a network model of BG-thalamocortical relations, which were used to provide a mechanistic account of the impairments found in PD handwriting. This computer simulation consists of a model of BG-thalamocortical relations in normal and PD conditions (Contreras-Vidal & Stelmach, 1995) and the VITE model (Bullock & Grossberg, 1988) of motor cortex (SMA, PM) for central pattern generation (CPG). The VITE model accounts for the trajectory formation, whereas the BG model acts as a movement gating and modulation mechanism. This model has been shown to reproduce many aspects of the normal and PD movement control, including hypometria, bradykinesia, akinesia, impairments in the coordination of multiple joints, micrographia, effects of L-dopa on movement size and speed, and pallidotomy. However, BG nuclei are modeled as lumped units, with activity levels represented by rate codes;

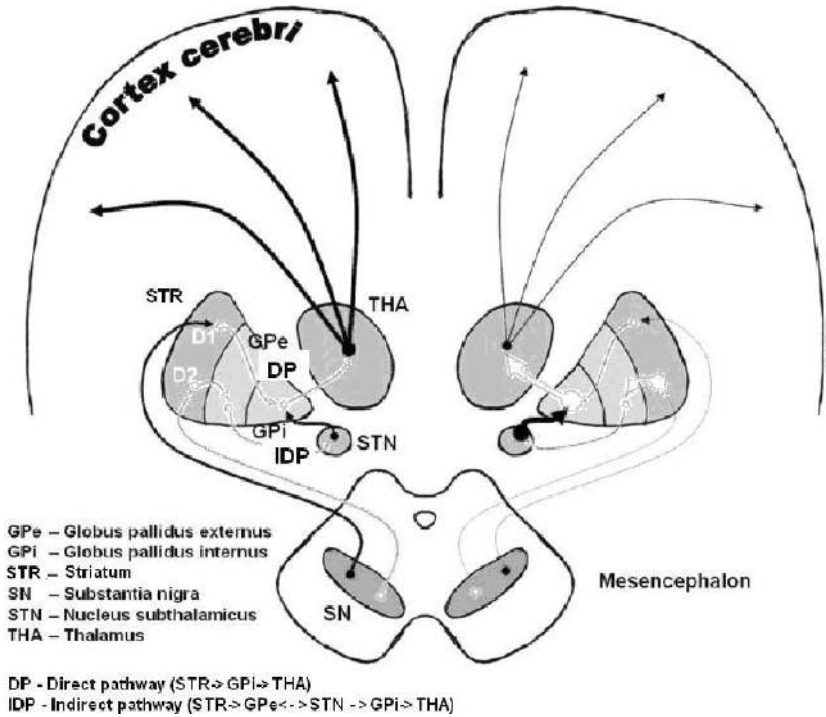

Figure 2: Dopaminergic pathways of the human brain in the normal condition (left) and Parkinson's disease (right). Light gray arrows indicate suppression of the target, and dark arrows indicate stimulation of target structure (figure adapted from www.wikipedia.com).

dynamic patterns in the activity of BG neurons are not accommodated. This is relevant because significant PD-related changes, particularly in the indirect pathway of BG, are found to occur not so much in terms of the rate code but more in terms of correlations among neural firing patterns (Terman, Rubin, Yew, & Wilson, 2002).

A key idea underlying the work presented here is to show that rhythm-related changes in PD that occur at the neuronal level can be used in a natural fashion to explain rhythm-related changes in PD like tremor as they manifest, for example, in handwriting.

1.4 Functional Architecture of BG: Relation to PD. Figure 2 shows the major nuclei and pathways that constitute BG during both normal and PD conditions. The striatum (STR) serves as a major target for the inputs from cortex to BG. Striatal output projections form two distinct parallel channels within the cortico-striato-pallidal pathways. The direct pathway is formed by the corticostriatal inhibitory projections from the neurons of striatal

output to neurons in the GPi. Activation of striatal neurons inhibits neurons in GPi, which in turn disinhibit thalamic nuclei. Conceptually the direct pathway can be seen as a normally closed movement gate that is opened by the corticostriatal activity that inhibits pallidal output allowing movement release. The indirect pathway is formed by corticostriatal inhibitory projections to GPe, which is thought to have an opposite effect to that of GPi neurons in the direct pathway. Corticostriatal activity in the indirect pathway tends to increase the activity of GPi cells and therefore closes the "gate" via disinhibition of thalamus. These pathways may be involved in modulating movement parameters (Contreras-Vidal & Stelmach, 1996).

Dopaminergic transmission from SNc has a differential effect on striatal neurons according to its receptor types, D1 and D2. The direct pathway is selected when D1 receptors are activated and the indirect pathway when D2 receptors are activated. Further, an increase in striatal dopamine shifts the balance toward the direct pathway, thereby increasing overall motor activity. Thus, the indirect pathway is the normally active pathway. The balance is switched just before movement onset, when dopamine release to striatum activates the direct pathway (Clark, Boutros, & Mendez, 2005).

An important conceptual breakthrough in functional understanding of BG came with the idea that dopamine (DA) release from the SNc, a BG nucleus, represents a reward signal, with the help of which rewarding responses to stimuli can be reinforced (Schultz, 1998). But the machinery for implementing reinforcement learning must consist, in addition to a reward signal, of a stochastic signal (the "explorer" component of reinforcement learning) that explores the space of possible responses. Although there have been models of exploratory behavior driven by dopaminergic neurons, neuroanatomical substrates of such exploration have not been addressed (Montague, Dayan, Person, & Sejnowski, 1995).

In an earlier work, we suggested that the complex activity present in the STN and the GPe is the explorer in BG (Sridharan, Prashanth, & Chakravarthy, 2006). It is known that under PD conditions, this natural complex activity degenerates into more regular forms of activity such as traveling waves or clustering (Terman et al. 2002; Bergman, Whichman, Karmon, & DeLong, 1994; Brown et al., 2001). Such highly regular, pathological activity of the STN-GPe system has been linked to PD tremor (Terman et al., 2002). There is also evidence that relates synchronized activity of pallidal neurons with PD tremor (Hurtado, Gray, Tamas, & Sigvardt, 1999). In this letter, we suggest, with the help of a model, that the nearly periodic, pathological activity of STN-GPe translates into aspects of distorted PD handwriting like jagged contour and abnormal fluctuations in velocity. PD has been dubbed a dynamical disease: neurons in the brain region associated with the disease operate in an abnormal dynamic regime (Beuter & Vasilakos, 1995). This letter is in tune with such a perspective of PD.

The letter is organized as follows. Section 2 presents a neuromotor model of handwriting generation in which stroke velocities are expressed

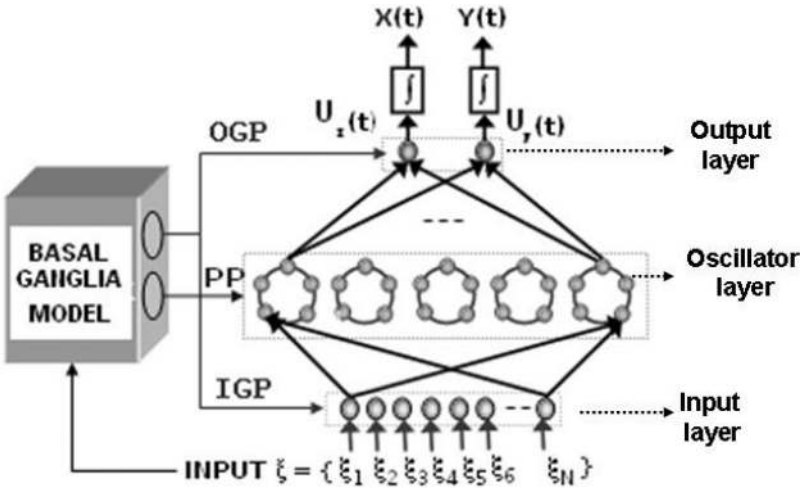

Figure 3: Architecture of the neuromotor model of handwriting generation. The stroke selection vector, ξ, is presented at the input layer. The outputs of the network are pen velocities, $U_x(t)$ and $U_y(t)$. The timing signals coordinate events in the network. It gates the input and output layers using input gate pulse and output gate pulse signals, respectively and prepares the oscillatory layer using the preparatory pulse signal. See the text for details.

as a Fourier–style decomposition of oscillatory neural activities. Aspects of network function like preparation of oscillator layer, timing, and training are discussed. Section 3 presents a model of BG, particularly highlighting the function of the indirect pathway consisting of the STN-GPe loop of BG. An integrated model consisting of the handwriting model of section 2, combined with the BG model of section 3, is presented in section 4. Various handwriting distortions that arise due to the introduction of PD pathology into the model are described in section 5. A coarse mapping of the integrated handwriting model and distortions in handwriting due to the PD pathological conditions is discussed in the section 6.

2 A Neuromotor Model of Handwriting Generation

The essence of the proposed approach to model handwriting generation is to produce a stable rhythm in a network of oscillators and resolve the stroke output in Fourier style in terms of the oscillatory activities of network oscillators (Gangadhar et al., 2007). The architecture of the network that learns to produce strokes has three layers: the input layer, the oscillatory layer, and the output layer (see Figure 3). The nodes in the input layer are stroke selection nodes (one node for each stroke). All the components of the

stroke selection vector (ξ) are set to zero in resting condition. To produce the kth stroke, for example, the stroke selection vector (ξ) is set as

$$\left.\begin{aligned} \xi_i(t) &= 1, \quad if\ i = k, \\ &= 0, \quad otherwise \end{aligned}\right\} \quad for\ t \in [0, T].$$

That is, the input node corresponding to the stroke is taken to a high value ($= 1$) and held at that value for a fixed duration, T. During the period ($t \in [0, T]$) when a given input node is in high state, velocity profiles ($U_x(t)$ and $U_y(t)$) of the corresponding stroke are generated at the output layer.

The oscillatory layer has several sublayers. All the neurons in a sublayer have the same oscillation frequency. In each sublayer, neurons are connected in a ring topology. All the neurons in the input layer are connected to all neurons in the oscillatory layer. The output layer has two outputs representing horizontal and vertical velocities (U_x and U_y) of the pen tip. All the neurons in the oscillatory layer are connected to both output neurons. Events in the three-layered network are controlled by the timing signals coming from the basal ganglia model. Equations of network dynamics are described below.

2.1 Single Oscillator Model. The dynamics of a single neural oscillator used in the oscillatory layer are given as:

$$\tau_x \frac{dx}{dt} = -x + V - s + I \tag{2.1}$$

$$V = \tanh(\lambda x) \tag{2.2}$$

$$\tau_s \frac{ds}{dt} = -s + V, \tag{2.3}$$

where V denotes the oscillatory output and x and s are auxiliary, internal variables of the neuron, respectively. Limit cycle oscillations are produced by the above system (see Gangadhar et al., 2007, for proof) but only within certain limits of the external input I (see Figure 4). Beyond those limits, the neuron has fixed-point behavior. The average output of the neuron as a function of I has a nearly sigmoidal form (see Figure 4). τ_x and τ_s are the time constants of equations 2.1 and 2.3.

2.2 Sublayer Model. Each sublayer consists of a network of oscillators (see equations 2.6, 2.7, and 2.8 below) connected in a ring topology. With a proper choice of parameters, such a network of oscillators can produce a limit cycle, with specific phase relationships among individual oscillators. An odd number of oscillators in a ring (sublayer) is preferred for mode locking because an even number of oscillators may lead to loss of rhythm

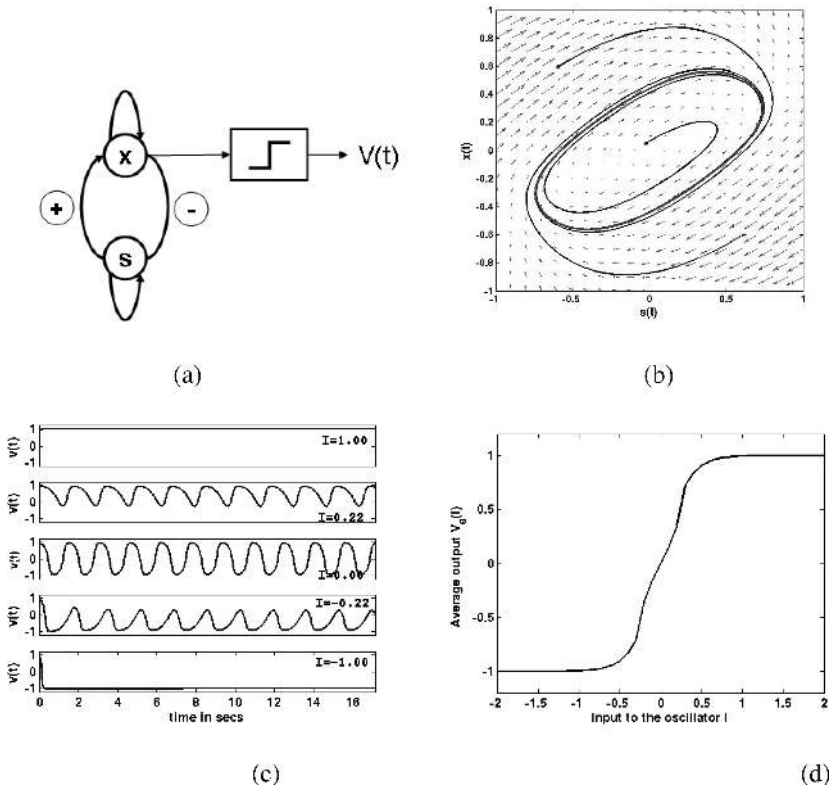

Figure 4: (a) Schematic depicting the dynamics of a single neural oscillator. Variable x excites s, which in turn inhibits x. x passed through a sigmoid yields V. (b) Dynamic flow of the system described by equations 2.1, 2.2, and 2.3 indicating the presence of a limit cycle attractor. (c) Response of a single neuron for various values of external input I (= 1.00, 0.22, 0.00, −0.22, −1.00, respectively, from top to bottom). (d) Average output response (V_a) of a single neuron as a function of I. The average is computed with simulations of oscillator over 100 cycles (= 100*120/70 secs, with 120 samples per cycle and sampling frequency of 70 hz) and 100 trials for each I with random initial values for x and s in the range [−1 1] (the parameters of the oscillator are $\tau_x = \tau_y = 0.24$ sec, $\lambda = 3$, the oscillatory regime for I in the range of [−0.25 0.25]).

stability, or "oscillator death" (Bressloff, Coombes, & Souza, 2002). A sublayer with a ring topology and an odd number of oscillators, where each oscillator is coupled with one (right or left only) neighbor with sufficiently strong (negative) coupling strength, exhibits mode locking, where each oscillator produces a periodic output and adjacent oscillators differ by a phase difference of $\Delta\phi = \pi + 2\pi/m$ (m is the number of oscillators) (Bressloff et al.,

2002). The period of oscillation of the oscillators can be varied trivially by scaling the two time constants, τ_x and τ_s (of equations 2.1 to 2.3) appropriately. All the oscillators in a sublayer are set to the same frequency. The sublayers themselves are set at harmonic frequencies $(f, 2f, 3f, \ldots)$, where f is the frequency of the first sublayer.

2.3 Network Model. Pen-tip velocities (U_x and U_y) estimated by the network are expressed as a weighted sum of the outputs of neurons in the oscillatory layer:

$$U_x(t) = \sum_{k=1}^{Ns} \sum_{i=1}^{Nk} W_{ik}^x V_{ik}(t) \tag{2.4}$$

$$U_y(t) = \sum_{k=1}^{Ns} \sum_{i=1}^{Nk} W_{ik}^y V_{ik}(t), \tag{2.5}$$

where N_s is the number of sublayers in the oscillatory layer and N_k is the number of oscillators in the kth sublayer, W_{ik}^x and W_{ik}^y are connections from the ith oscillator in the kth sublayer to output nodes U_x and U_y, respectively. Output V_{ik} of the ith oscillator in the kth sublayer is given by

$$\tau_x \frac{dx_{ik}}{dt} = -x_{ik} + \sum W_{irk}^{lat} V_{rk} - s_{ik} + I_{ik}^{net} \tag{2.6}$$

$$V_{ik} = \tanh(\lambda x_{ik}) \tag{2.7}$$

$$\tau_s \frac{ds_{ik}}{dt} = -s_{ik} + V_{ik}, \tag{2.8}$$

where x_{ik} is the state of the ith neuron in the kth sublayer, s_{ik} is the auxiliary internal variable of the ith oscillator in the kth sublayer, and W_{irk}^{lat} is the lateral connection from the rth oscillator to the ith oscillator in the kth sublayer. As described earlier, each sublayer is a ring in which oscillators are connected in a unidirectional fashion with negative coupling strengths as follows:

$$\begin{aligned} W_{irk}^{lat} &= \nu; \quad if\ (r = i+1),\ or\ (r = 1\ \&\ i = N_k) \\ &= 0, \quad otherwise. \end{aligned} \tag{2.9}$$

In the simulations in the following section, we take $\nu = -0.5$. I_{ik}^{net} as the net input to the ith oscillator in the kth sublayer, given by

$$I_{ik}^{net} = \sum_l W_{ik}^{1l} \xi_l, \tag{2.10}$$

where ξ_l is the lth input in the input vector $\xi = \{\xi_1, \xi_2, \xi_3, \ldots, \xi_l, \ldots, \xi n, -1\}$ and W_{ik}^{1l} is the weight connecting the lth input node and the ith oscillator in the kth sublayer. The last component of ξ, -1, is the bias input to the oscillatory layer, and the corresponding weight is set to $+1$. We now describe various functional aspects of handwriting generation.

2.4 Preparing the Network State. This important stage is described variously in literature as system configuration, motor programming, coordinative structure gearing, preparation, planning, and schema buildup (Schomaker, 1991). We use the term *preparation* in this letter. Although the problem of motor preparation has several dimensions, in the context of our network model, we give it a specific meaning. Since the oscillatory layer is a dynamic layer, it must be initialized appropriately before every stroke execution for reliable learning. A simple form of initialization is to set the oscillatory layer to a standard state, say, V^s. But this initialization cannot arbitrarily be done programmatically. We define auxiliary dynamics, which drives the oscillatory layer toward the standard state, V^s. This process, termed *preparation,* is achieved by giving a preparatory pulse (PP) to a specific neuron (chosen to be the first neuron in every sublayer without loss of generality) and waiting for a specific delay interval. The delay must be long enough to allow the oscillatory layer state to approach the predetermined state, V_s, in the limit cycle sufficiently closely. Since the oscillatory layer has a limit cycle attractor, once the steady state is reached, the oscillatory layer, in free-running conditions (no external input), periodically visits every point on the limit cycle. The standard state is chosen to be a point on the limit cycle. We define the standard state, V^s, as the state reached by the oscillatory layer at the end of a specific preparatory delay (time elapsed after the PP), Δ (600 time units), and with a specific PP of duration, τ (20 time units) and amplitude, A (20). PP is given as an external input, I_{ik}^{net}, in equation 2.6. PP is a rectangular pulse of amplitude, A, and duration, τ, given to the first neuron in each sublayer. (See Gangadhar et al., 2007, for a more detailed depiction of preparatory dynamics.)

2.5 Timing Signals. BG nuclei are thought to be involved in a variety of timing functions (Buhusi & Meck, 2005). In the model here, the timing signals (see Figure 5) from the BG model control the timing of various events in the handwriting network (see Figure 3). The command to execute a stroke corresponding to the jth node in the input layer, is received by the handwriting network at $t = 0$ ms (event A). Immediately (at $t = 0 +$ ms), PPs (of duration τ) are sent to a single (first) neuron in each of the sublayers of the oscillatory layer. The end of PPs marks event B. The network is then allowed to oscillate freely until it reaches a standard state (as described in the previous paragraph) for a delay of Δ ms. After this delay, enabling signals, input gate pulse (IGP) and output gate pulse (OGP), are sent to the input layer and output layer, respectively. OGP modulates the velocity

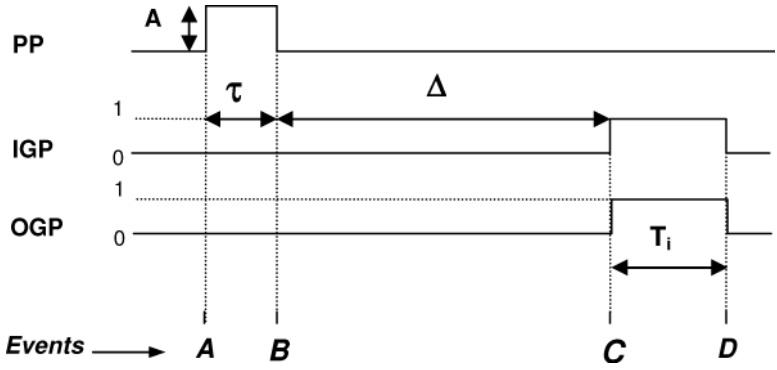

Figure 5: The timing signals (PP: preparatory pulse, IGP: input gate pulse, OGP: output gate pulse). A is the amplitude of preparatory pulse, τ is the duration of PP, T_i is the duration of OGP for the ith stroke, which is currently the same, T_f, for all strokes. See Table 1 for a summary of events A, B, C, and D.

Table 1: Summary of Events in Handwriting Generation.

Events	Event Summary
A	The input is fed to the handwriting network (also to the BG model). The BG model injects PP for the duration ($\boldsymbol{\tau}$), to the first oscillator in every sublayer. Input to the oscillatory layer is disabled during this interval since the IGP is low.
B	This event is the end of PP and the start of preparatory delay for duration Δ. IGP and OGP continue to be low.
C	Start of IGP and OGP with duration $\boldsymbol{T}_i$, which enable the input and output. The handwriting network starts generating velocity information.
D	The end of IGP and OGP; the handwriting network output is again disabled, velocities become 0, and the pen tip stops.

output of handwriting network (when OGP $= 0$, both velocities are 0; when OGP $= 1$, the velocities are available, and execution begins). At the start of event C, the execution of the handwriting begins. The gating duration, from event C to event D, T_i, generally must be specific to the stroke that is being produced (see Figure 5). However, we consider a simpler situation where all strokes are of equal duration, which is equal to the time period, T_f, of the slowest oscillators (those of first sublayer) in the oscillatory layer. (See Table 1 for a summary of events A, B, C, and D.)

A single movement consists of two stages: preparation and execution. A PP signal is given at the beginning of preparation. Preparation ends when the network approaches the standard state, V_s, at which time OGP is turned

ON (1) and execution begins. Execution ends when OGP is turned off after a fixed duration.

2.6 Training. Since the time-averaged output of the oscillatory neuron varies in a sigmoid form as a function of external input (see Figure 4), a backpropagation (BP) algorithm may be used for training (Haykin, 1998). Backpropagation with momentum and without momentum (plain BP) (Haykin, 1998) are tried for training the handwriting model. The BP algorithm is normally used to train a multilayered perceptron to map static input-output vector pairs. In the present case, the oscillatory network is trained to produce time-varying stroke velocities as follows. To train the network on the lth stroke, ξ_l, the lth input component in input vector $\xi = \{\xi_1, \xi_2, \xi_3, \ldots, \xi_l, \ldots, \xi n, -1\}$, is set to 1, and all other input components are set to 0. The corresponding target output is a sequence of stroke velocities, $V_x(t)$ and $V_y(t)$. Note that the oscillatory layer is prepared as described earlier and brought close to the standard state before training every stroke. Since time is discretized, when the network is trained to produce a stroke, it is actually trained to map the following sequence of input-output pairs:

$$\xi(t_m) \rightarrow (V_x(t_m), V_y(t_m)),$$

where $\xi(t_m) = \xi$ (input is constant throughout the stroke) and t_m is the mth instant. Only the first (W_{ik}^{1l} for all l, i, and k in equation 2.10) and second-stage weights (W_{ik}^{x} and W_{ik}^{y} for all i and k in equations 2.4 and 2.5) are trained; the lateral weights (W_{irk}^{lat} in equation 2.9) in the oscillatory layer are constant. Weight update equations are as in Haykin (1998). A comparison of training error corresponding to learning algorithms plain BP and BP with momentum is shown in Figure 6.

2.7 Calculation of Mean Error. The mean error shown in Figure 6 is calculated using the formula

$$E = \sum_{p}^{N_S} \sum_{q}^{N_L} \left\{ \left(V_x^{pq} - U_x^{pq}\right)^2 + \left(V_y^{pq} - U_y^{pq}\right)^2 \right\}, \tag{2.11}$$

where V_x^{pq} and U_x^{pq} are the qth points in the desired and actual x-velocities of the pth stroke, respectively. Similarly, subscript y indicates y-velocity. E is the average reconstruction error in stroke velocity, N_S is the number of strokes, and N_L is the number of points in velocity profile of a stroke, which is the same for all strokes (Gangadhar et al., 2007).

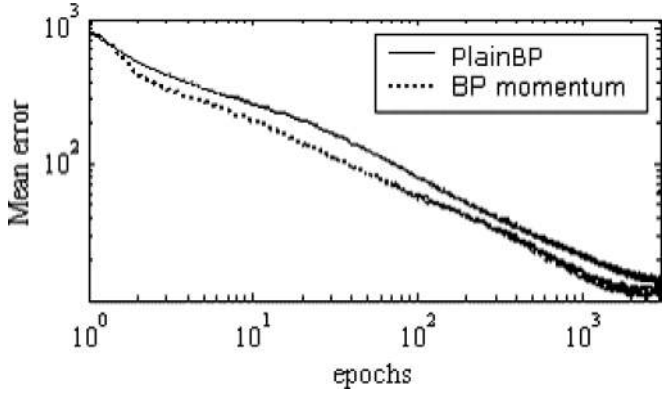

Figure 6: Comparison of training error corresponding to learning algorithms plain BP and BP with momentum. The mean error for BP with momentum converges faster than the plain BP learning mechanism. An epoch means a single presentation of all strokes.

3 A Model of Basal Ganglia

We noted in section 1 that at elevated striatal dopamine levels, striatopallidal transmission switches from the indirect pathway under resting conditions, to the direct pathway, thereby initiating movement. In dopamine-deficient conditions of PD, it is probable that such a transfer may not occur effectively; under such abnormal signaling conditions, activity of the indirect pathway may then contribute significantly even during movement, introducing distortions like tremor and velocity fluctuations. Therefore, a model of BG under dopamine-deficient PD conditions will necessarily be dominated by the indirect pathway. Here we describe a model of the STN-GPe, a subsystem of BG, that constitutes the indirect pathway. Since the indirect pathway is overactive PD conditions, we present a model of this pathway as a complete model of BG in PD conditions.

A single STN-GPe neuron pair with glutamergic (+) and GABAergic (−) connections is shown as excitatory and inhibitory connections in Figure 7a. The dynamics of a GPe neuron is given by

$$\tau_g \frac{dx_{GPe}}{dt} = -x_{GPe} + U_{GPe} + x_{STN} + I_{GPe} \tag{3.1}$$

$$U_{GPe} = \tanh(\lambda x_{GPe}), \tag{3.2}$$

where U_{GPe} denotes the output of the GPe neuron with its internal state x_{GPe}, I_{GPe} is the external input to the GPe neuron, x_{STN} is the state of the STN neuron, τ_g is the time constant, and $\lambda(\gg 1)$ controls the slope of tanh

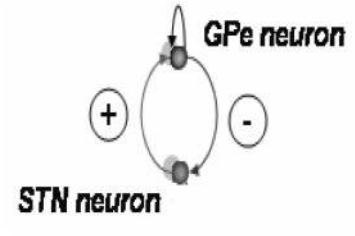

(a)

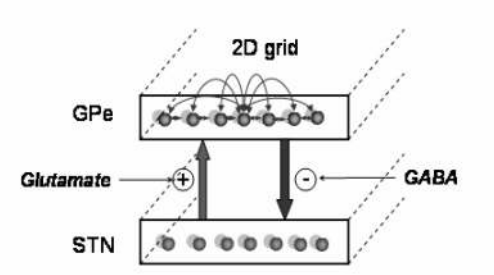

(b)

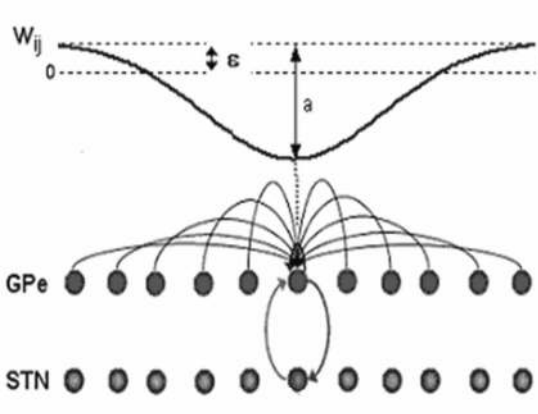

(c)

Figure 7: (a) STN-GPE neuron pair showing exitatory and inhibitory connections. (b) Grid of STN-GPe networks. (c) Strengths of the lateral connections in the GPe network, with a as the height of the inverted gaussian, ε, as the positive bias to it.

function. Similarly, the dynamics of STN neuron is given by

$$\tau_s \frac{dx_{STN}}{dt} = -x_{STN} - U_{GPe}, \tag{3.3}$$

where τ_s is the time constant. Note that while U_{GPe} has an inhibitory influence on x_{STN}, x_{STN} in turn excites U_{GPe}. U_{GPe} can vary between $+1$ and -1 depending on the terms on the right-hand side of equation 3.1. Since x_{STN} is driven by U_{GPe} per equation 3.3, x_{STN} varies between $+1$ and -1 (through equation 3.3). The outputs, U_{GPe} and x_{STN}, of GPe and STN neurons, respectively, denote the deviations from baseline firing rates of the respective neurons. Note that the dynamics of equation 3.3 is slower than the dynamics of equation 3.1. Oscillations are produced by the above system, but only within certain limits of the external input I_{GPe}. Such two-variable models of STN-GPe dynamics have been proposed earlier (Gillies, Willshaw, & Li, 2002).

The pair of neurons described above is replicated and connected in a 2D grid fashion for realizing the STN-GPe loop as shown in Figure 7b. The connections between these nuclei are assumed to be one-to-one with inclusion of lateral connections in the GPe layer and no lateral connections in the STN layer. Lateral connections of the GPe layer are calculated using equation 3.7 (see Figure 7c). Each of these layers is implemented in a 2D grid fashion, and the dynamics of the layers are given by

$$\tau_g \frac{dx_{ij}^{GPe}}{dt} = -x_{ij}^{GPe} + \sum_{q=1}^{n}\sum_{p=1}^{n} W_{ij,pq}^{lat} U_{pq}^{GPe} + x_{pq}^{STN} + I_{ij}^{GPe} + I_{ij}^{DA} \tag{3.4}$$

$$U_{ij}^{GPe} = \tanh\left(\lambda x_{ij}^{GPe}\right) \tag{3.5}$$

$$\tau_s \frac{dx_{ij}^{STN}}{dt} = -x_{ij}^{STN} - U_{ij}^{GPe}, \tag{3.6}$$

where (i, j) and (p, q) denote two neuron positions on the 2D grid, n is the size of the 2D grid, x_{ij} is the internal state of the (i, j)th neuron on the GPe grid, x_{ij}^{STN} is the state of the (i, j)th neuron on the STN grid, U_{ij}^{GPe} is the output of the (i, j)th neuron on the GPe network, and I_{ij}^{DA} is the input to the (i, j)th GPe neuron to account for the indirect effect of striatal dopamine on the activity of neurons of STN-GPe layer. The lateral connections within the GPe layer (see Figure 7c) are assumed to be translation invariant and are given by

$$\begin{aligned} W_{ij,pq}^{lat} &= \varepsilon - a \exp\left(-r_{ij,pq}^2/\sigma_{lat}^2\right) \qquad \text{for } r < R \\ &= 0, \text{ otherwise,} \end{aligned} \tag{3.7}$$

where $r_{ij,pq} = [(i-p)^2 + (j-q)^2]^{1/2}$, is the squared distance between neurons at locations (i, j) and (p, q), respectively, on the 2D grid; a is a positive number that controls the depth of the gaussian bell function, σ_{lat} is its width, and R is the neighborhood size. Thus, each unit has a negative center and a positive surround; the relative sizes of center and surround are determined by ε. Smaller ε implies more negative lateral GPe connections. In the absence of input from the input layer ($I_{ij} = 0$), as ε is varied from 0 to a, the activity of STN-GPe system varies from uncorrelated behavior to highly correlated behavior.

The quantity I_{ij}^{DA} introduced in equation 3.4 denotes the indirect effect of striatal dopamine on the activity levels of GPe neurons. Model dynamics are designed such that the fraction of active neurons in GPe is proportional to DA. For example, note that in Figure 8a, where $DA = 50$, at any instant approximately 50% of the GPe neurons are in an active state. Similarly, in Figure 9a, where DA = 20, at any instant approximately 20% of the GPe neurons are in an active state. This control is achieved by the following feedback control mechanism:

$$\nu^{total} = \frac{1}{2}\sum_{i,j}^{N}\left(U_{ij}^{STN} + 1\right) \tag{3.8}$$

$$e = DA - \nu^{total} \tag{3.9}$$

$$\tau\frac{dE}{dt} = \tanh(\lambda_g * e) \tag{3.10}$$

$$I_{ij}^{DA} = E - \frac{N}{2}, \tag{3.11}$$

where ν^{total} is the actual number of total active units, N is the number of neurons in the GPe (and also the STN layer since the two layers are connected one-to-one), and e denotes the discrepancy between the actual number of active units, ν^{total} and DA levels, at a given instant. The discrepancy is accumulated in E. The parameter λ_g (= 10) controls the slope of the tanh function, and τ is the time constant of feedback dynamics (see equation 3.10). I_{ij}^{DA} is the input to the GPe neuron, as shown in equation 3.4.

In equation 3.9, e denotes the error—the difference between the desired number of active GPe neurons and the actual number of active GPe neurons. E is approximately an integrated version of the error e. When E is large positive, I_{ij}^{DA} tends to activate GPe neurons; when E is small positive or negative, I_{ij}^{DA} tends to deactivate GPe neurons. The negative bias ($-N/2$) in equation 3.11 ensures that all GPe neurons are inactive when $E = 0$.

Figure 8 shows the temporal evolution of the STN-GPe system in the three dynamic regimes. For a fixed DA(50), as ε is increased from 0, the STN-GPe system transitions systematically from complex activity ($\varepsilon < 0.1$)

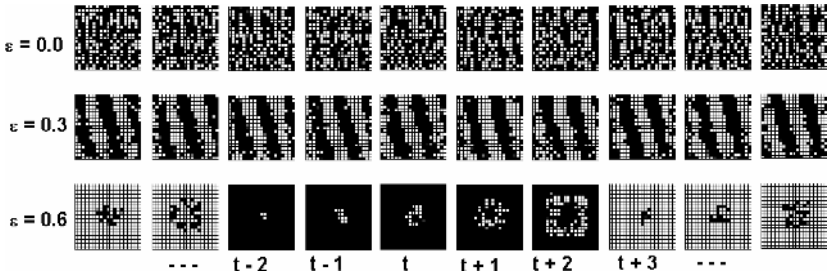

Figure 8: Snapshots of GPe network activity over time for the values of $\varepsilon = 0.0$, 0.3, and 0.6. The black square corresponds to negative and the white square to positive values. We can observe the complex activity regime for $\varepsilon = 0.0$, traveling waves for $\varepsilon = 0.3$ (observe the third black stripe moving from left to right as wave), and synchronized cluster activity for $\varepsilon = 0.6$. The GPe layer size is 20×20 (DA $= 50$).

to traveling waves ($0.1 \leq \varepsilon < 0.5$), to synchronized cluster ($\varepsilon \geq 0.5$) (see Figure 8). In the synchronized cluster regime (the bottom row of Figure 8), a group of neurons in the center fire in synchrony but out of synch with all the other neurons. Thus, at any given instant, a large number of background neurons are in a synchronized state. Similar dynamical regimes are observed in the electrophysiological model of STN-GPe studied by Terman et al. (2002). Terman et al. relate the regular dynamic regimes (traveling waves and clusters) to the tremor-like symptoms of Parkinsonism. Therefore, we associate the first regime (complex activity) with normal function and the other two (traveling waves and synchronized cluster) with PD pathology. The changes in dynamics can also be seen clearly in the two-dimensional fast Fourier transform (2D-FFT) shown in Figure 9 (DA $= 50$). The FFTs corresponding to the complex activity regime are rather diffuse; as the dynamics transition to traveling waves, two sharp peaks appear in the FFT denoting the (approximate) spatial periodicity seen in activity in this regime. When the system is in a synchronized cluster regime, the FFT shows only a single peak.

However, for DA $= 20$, the variety of dynamic behaviors seen in the case of DA $= 50$ are not observed, probably because there are too few active neurons at any given instant in this case (see Figure 10). Thus for a fixed DA, increasing ε increases regularity in STN-GPe dynamics. The transition from complex dynamics to regular dynamics is abrupt for larger values of DA and smoother for smaller DA values (see Figure 10).

We quantify the behavior of the STN-GPe system using the measure of average pairwise correlation (APC) (see Figure 11 for APC simulation for $DA = 20$ and 50). To compute APC, correlations between activities of pairs of GPe neurons are calculated; the average value of those correlations is the

ε	Snapshot of STN grid	FFT of the STN activity
0.0	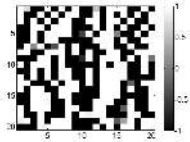	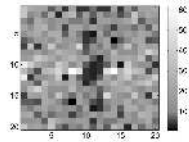
0.1		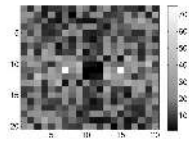
0.2	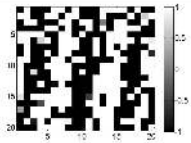	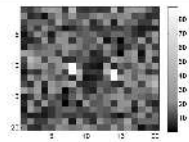
0.3	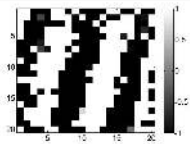	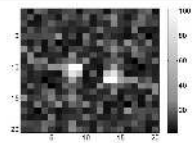
0.4		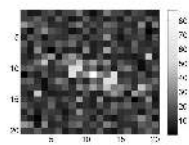
0.5	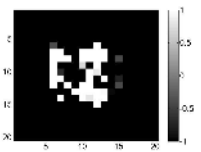	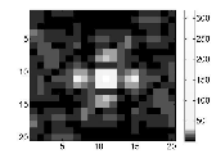
0.6	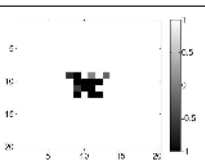	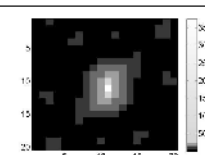

APC. We can observe a sudden rise in the APC for the case of DA = 50 after $\varepsilon = 0.4$ due to switching the STN-GPe system into a synchronized cluster (see Figures 11 and 9). For DA = 20, the APC increases more smoothly than in the previous case.

Thus, in this section, we presented a PD model of basal ganglia in which only the indirect pathway is highlighted, since the direct pathway normally remains unselected under dopamine-deficient conditions. Two control parameters—striatal dopamine (DA) and GPe connectivity (ε)—determine the nature of STN-GPe dynamics in the model. Normal conditions are associated with DA = 50 and $\varepsilon = 0$. PD pathology is induced by reducing DA or increasing ε from these normal values. Reducing DA (<50) reduces the activity levels of GPe layer; increasing ε(>0) pushes the STN-GPe dynamics to more regular regimes (traveling waves and synchronized clusters). We now present the integrated model by combining the neuromotor system and BG to study handwriting in both normal and PD conditions.

4 Integrating Models of Basal Ganglia and Neuromotor System

The BG model with its indirect pathway (described in section 3) is integrated with the neuromotor model of handwriting generation (described in section 2) for understanding Parkinsonion handwriting. The output of the BG model modulates the stroke velocities arising from the handwriting model. The generation of timing signals (PP, IGP, and OGPs) of BG's indirect pathway is not modeled explicitly with a network in this letter. They are simply specified as in Table 1. Only the activity of the indirect pathway is modeled in the network structure described in section 3. A conceptual schematic of the integration is depicted in Figure 12.

The event sequence of the integrated handwriting model during the execution of a single stroke is:

1. The initial settings. The IGP is set to zero, so that input (ξ) cannot affect the oscillator layer of handwriting model before it is prepared. Also the OGP_x and OGP_y are set to zero, so that the velocity of the pen

Figure 9: Dynamics of the STN-GPe loop. The snapshots of the STN layer are shown in column 2 for various values of ε. The activity regimes (from top to bottom) are obtained by progressively increasing ε from 0 to 0.6, keeping the DA value at 50. Increasing ε increases the percentage of positive lateral connections in STN (a black square means negative values and a white square positive values). In column 3, the centered magnitude spectrum of the two-dimensional FFT of the STN-GPe activity is shown. Note the prominent peaks along the x-axis for $\varepsilon = 0.3$. These peaks in magnitude occur at the frequency corresponding to that of the traveling wave (STN layer size is 20×20).

ε	Snap shots of STN grid	2D-FFT of STN activity
0.0	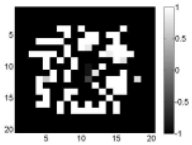	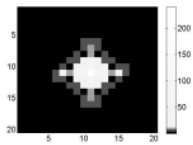
0.1	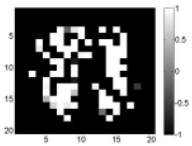	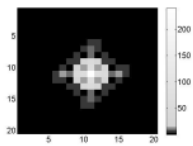
0.2	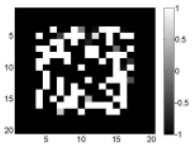	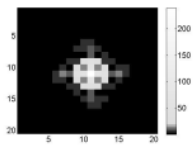
0.3	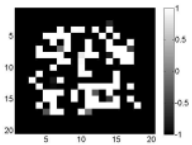	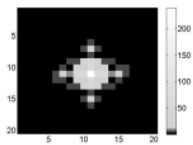
0.4	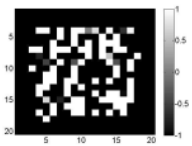	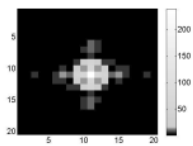
0.5	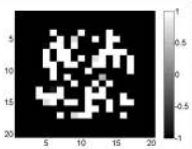	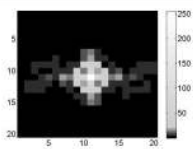
0.6	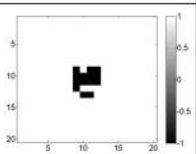	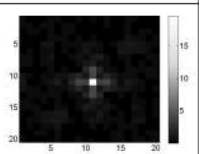

tip is maintained at zero (the pen tip does not move; this represents the action gating function of BG).

2. Motor preparation. On the arrival of stroke selection input at the neuromotor model in Figure 12, a copy of the same is sent to the BG model, which then sends a preparatory signal (PP) to the oscillator layer, shown in Figure 3.
3. Stroke execution. Once the preparation is complete, the BG allows the OGP_x and OGP_y to vary according to the activity of the STN-GPE system. The OGP_x and OGP_y signals modulate the output of the neuromotor model. These velocities are integrated to get the current pen position. Once the stroke generation is complete, the stroke selection input (ξ) to the model is reset. This resets the values of IGP, OGP_x, and OGP_y (low or zero).

Thus, the signals arising from the indirect pathway of BG modulate the velocity signals of handwriting model as follows:

$$U_x(t) = OGP_x(t) \sum_{k=1}^{N_s} \sum_{i=1}^{N_k} W_{ik}^x V_{ik}(t) \tag{4.1}$$

$$U_y(t) = OGP_y(t) \sum_{k=1}^{N_s} \sum_{i=1}^{N_k} W_{ik}^y V_{ik}(t), \tag{4.2}$$

where

$$OGP_x(t) = \sum_{i=1}^{n} \sum_{j=1}^{n} W_{ij}^{STN_x} U_{ij}^{STN}(t) \tag{4.3}$$

$$OGP_y(t) = \sum_{i=1}^{n} \sum_{j=1}^{n} W_{ij}^{STN_y} U_{ij}^{STN}(t), \tag{4.4}$$

where $W_{ij}^{STN_x}$ and $W_{ij}^{STN_x}$ are the weights connecting STN neurons to the GPi nodes $OGP_x(t)$ and $OGP_y(t)$, respectively.

Figure 13 shows the event sequence and corresponding outputs of the integrated model under normal and PD conditions. Observe the kinky nature of the stroke under PD conditions. In the next section, we report results of the experiments conducted on the integrated model.

Figure 10: Dynamics of the STN-GPe loop. The patterns of activity of the STN layer are obtained by increasing ε from 0 to 0.6 and correspond to a DA level of 20. In column 2 a snapshot of STN activity is shown. In column 3, the centered magnitude spectrum of the two-dimensional FFT of the STN layer activity is shown (observe the gray-scale bar). The size of the STN layer is 20×20.

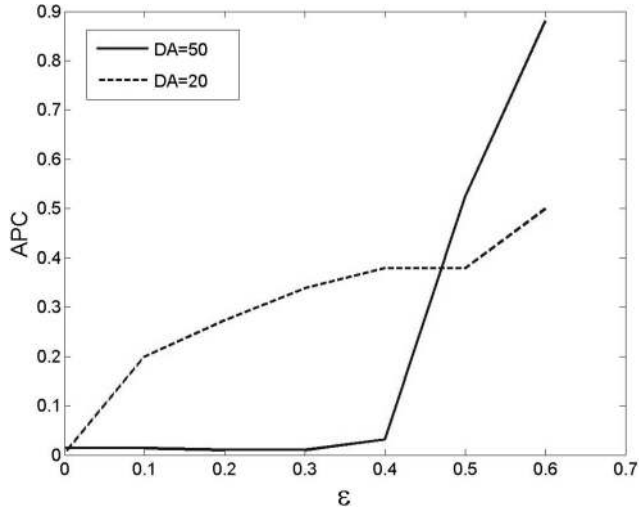

Figure 11: Variation in APC by progressively increasing ε from 0 to 0.6 (DA = 50, solid line; DA = 20, dashed line).

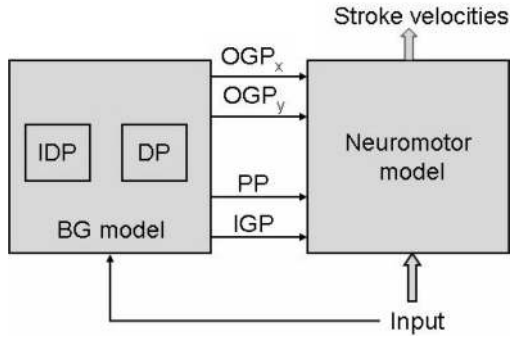

Figure 12: Conceptual schematic of the integrated BG and neuromotor model for generating handwriting. BG—basal ganglia; IDP—indirect pathway; DP—direct pathway; PP—preparatory pulse; IGP— input gate pulse; OGP$_x$—output gate pulse for stroke velocity along the x-axis; OGP$_y$—output gate pulse for stroke velocity along the y-axis.

5 Results

Lowercase English alphabets are collected using a stylus and electronic pen (Graphire tablet) connected to a computer. These strokes are represented by pen-tip coordinates, $x(t)$ and $y(t)$, along the x-direction and y-direction, respectively. The sampling frequency of the device is 70 Hz, and hence

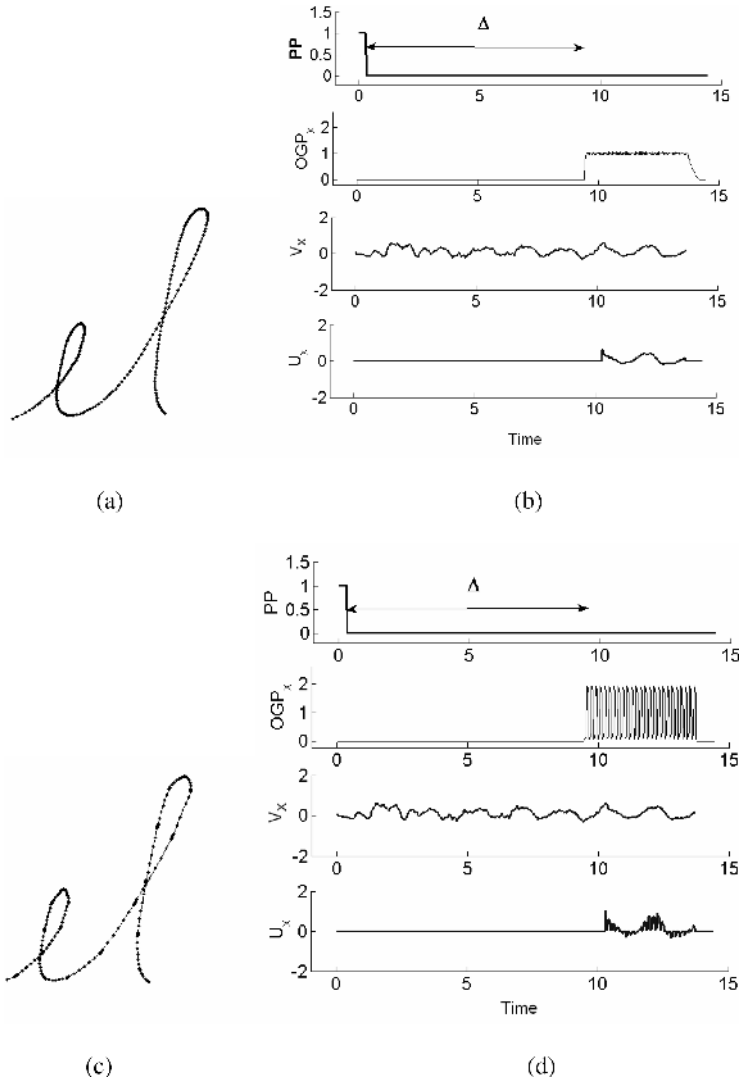

Figure 13: Event sequences during the execution of handwriting with the integrated model. PP is preparatory pulse; OGP_x is the output gate pulse for the U_x output node; V_x is the actual velocity (weighted sum of oscillator layer activity) profile at node U_x in Figure 12; U_x is the modulated velocity profile (computed using equation 4.1); Δ is the preparation delay. (a) Handwriting generated with normal conditions (DA $= 50$, $\varepsilon = 0.0$). Observe the smooth profile of the strokes. (b) Event sequence during the execution of the word *el* under normal conditions. (c) Handwriting generated with impaired conditions (DA $= 50$, $\varepsilon = 0.55$) similar to PD. Observe the kinky profile of the strokes. (d) Event sequence during the execution of the word *el* under PD conditions.

the sampling time (referred to as the time unit in this letter) is equal to 1/70 seconds. The strokes collected are nearly of uniform length; points toward the end are dropped to make all the strokes are equally long (120 points per stroke). The height of each stroke written on the track pad is around 1 cm. The duration (T) of each stroke is therefore $120 * (1/70) = 1.7143$ seconds. The strokes are used to train the handwriting model. The frequency of sublayer with the lowest frequency of oscillations is set to $f = 1/T$. Training is performed using BP with momentum. Learning rates for the first- and second-stage weights are 0.000005 and 0.0001, and the momentum factor is 0.7 (refer to Gangadhar et al., 2007, for detailed results of the neuromotor model of handwriting generation). We now study the effects of deviations from normal values of DA and ε (DA = 50 and $\varepsilon = 0$) on the handwriting generated by the model.

5.1 Simulation Experiment 1. The trained network is instructed to write the word *el* with the value of DA kept constant at 50 throughout the experiment and the value of ε varied from 0.0 to 0.6 in steps of 0.1 across trials. The output of the network is collected together with a time series of values corresponding to the magnitude of the velocity vector. The standard deviation of these values is also computed (see Figure 14).

Higher ε value produces synchronized oscillations in the STN-GPe system. These synchronized oscillations induce fluctuations in the output of GPi, which is simply the OGP (see Figure 14). Since OGP modulates both GP_x and GP_y the resulting handwriting has a jagged contour and is marked by abnormal fluctuations in the velocity profile. The variation in the standard deviation of the magnitude of the velocity of the pen tip as a function of ε is shown in Figure 15. The standard deviation increases with increasing ε and shoots up rapidly after $\varepsilon = 0.4$.

5.2 Simulation Experiment 2. In this experiment, we systematically vary the values of both parameters, DA from 10 to 50 and epsilon from 0.0 to 0.6, over different trials (see Figure 16). The output of the network as a function of DA and ε is shown in Figure 16.

The results of this experiment allow us to map the handwriting features onto the level of PD, which, we suggest, can be parameterized by the level of dopamine (DA) and the level of distortion in STN-GPe activity, controlled by ε. The output of the network clearly demonstrates that as dopamine is decreased, the overall size decreases (micrographia); as ε is increased, stroke contour becomes more and more jagged, and the velocity profile manifests large fluctuations. This is in line with the characteristic features of handwriting observed in a PD patient: reduced stroke size, jagged handwriting, and velocity fluctuations.

5.3 Simulation Experiment 3. In this experiment, we vary both DA and epsilon over their respective ranges, but on a finer scale. We chose

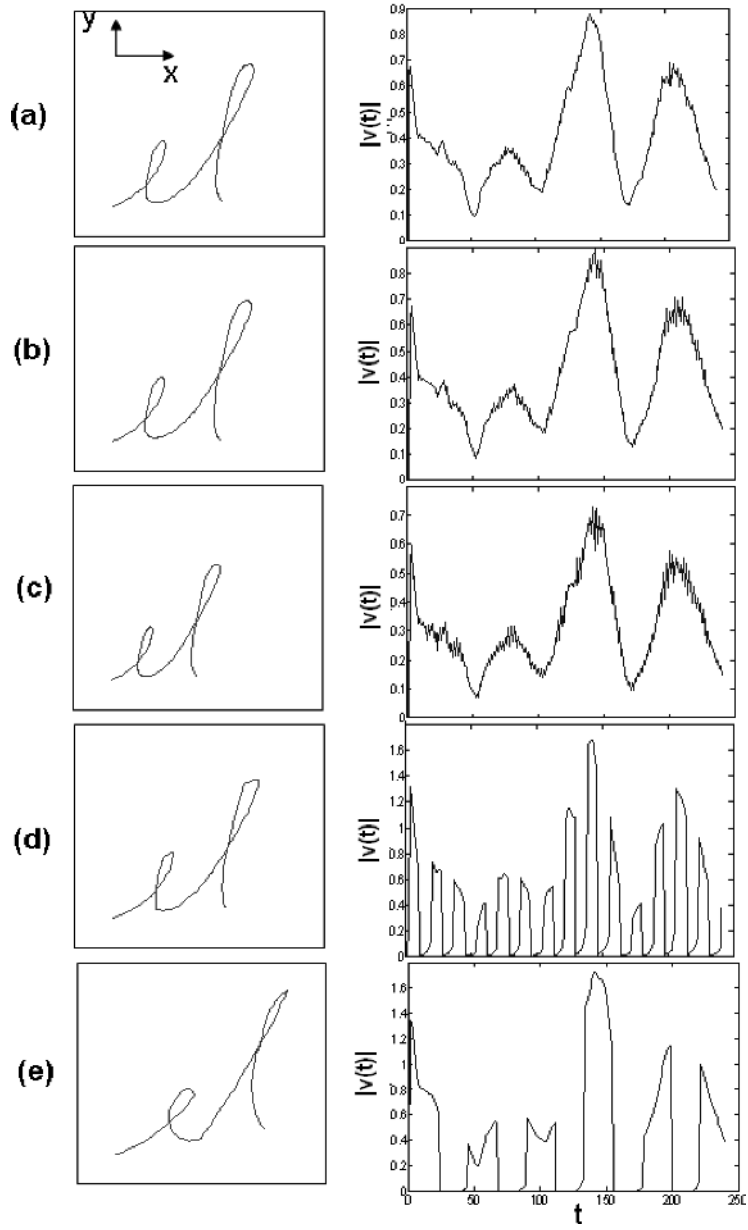

Figure 14: The output stroke sequence generated by the network in the left column and the magnitude of the velocity (1 unit is equal to 3 cm/sec) of the pen tip in the right column with a DA level of 50 with values of ε is varied. The pen velocity magnitudes for various values of epsilon are as indicated: (a) $\varepsilon = 0.0$, (b) $\varepsilon = 0.2$, (c) $\varepsilon = 0.4$, (d) $\varepsilon = 0.6$, (e) $\varepsilon = 0.8$.

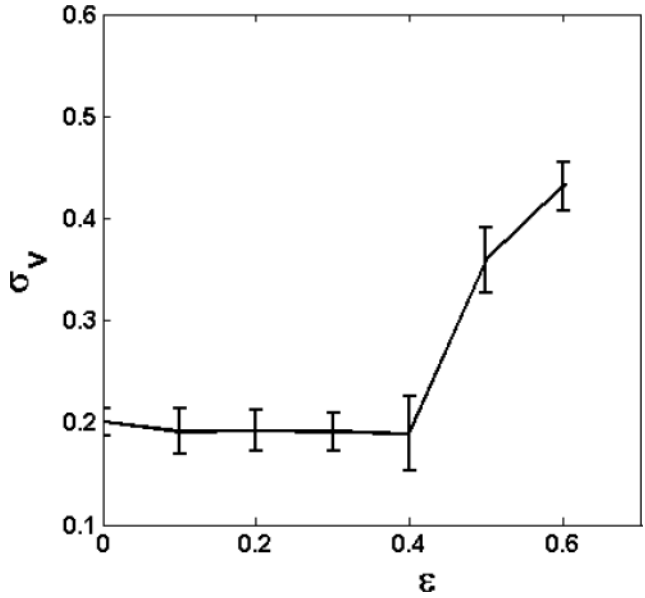

Figure 15: Variation in the standard deviation of the magnitude of the velocity of the pen tip as a function of ε. On the y-axis, one unit is equal to 3 cm/sec.

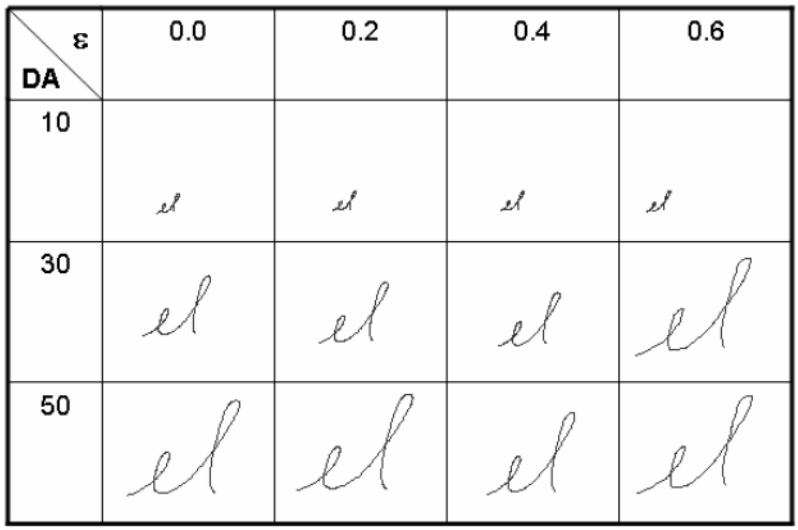

Figure 16: The output of the model for various values of ε and DA. Horizontally from left to right, ε is varied from 0.0 to 0.6; vertically from top to bottom, DA is varied from 10 to 50. As the value of DA decreases, the stroke size decreases.

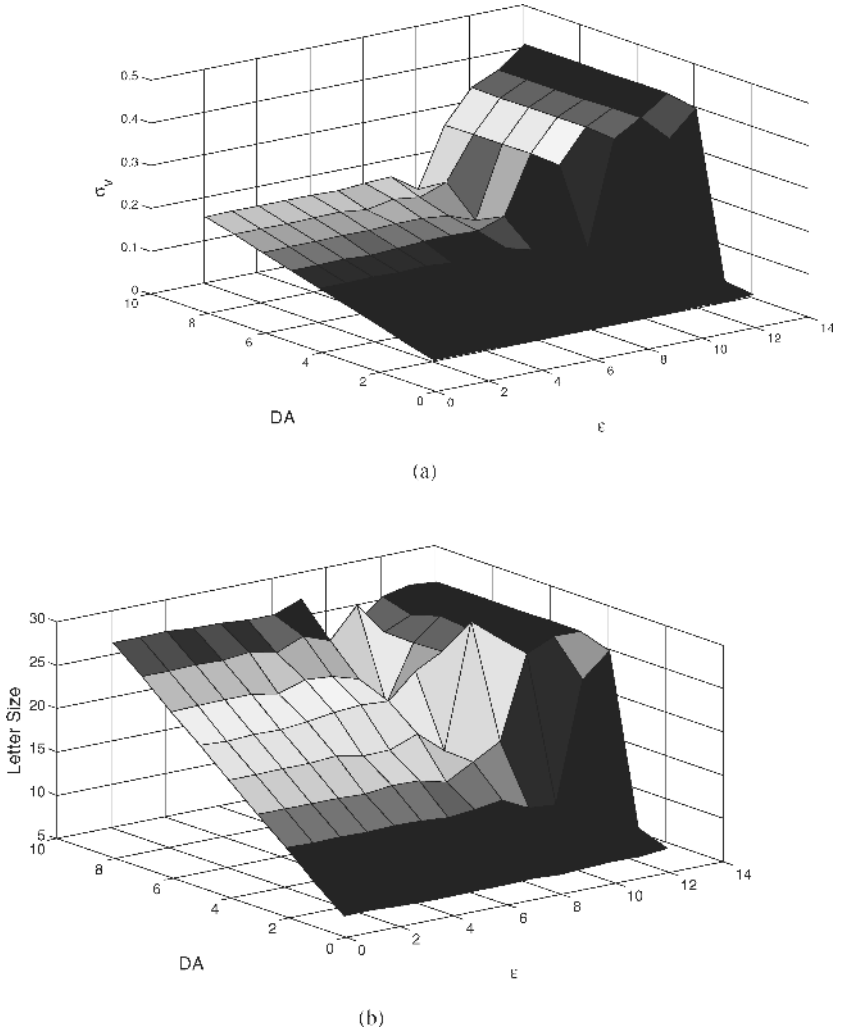

Figure 17: The figures show how the two metrics, (a) σ_v (one unit = 30 mm/sec) and (b) LS, vary as a function of DA and ε.

two metrics and analyzed their behavior over the range of values that DA and ε assume. The metrics are standard deviation of the magnitude of the velocity, σ_v, and letter size (LS), which we chose as the height of the letter l, without loss of generality. The metrics vary in a complicated fashion over the space of parameters that represent PD pathology (see Figure 17).

5.4 Simulation Experiment 4: Progressive Micrographia. Micrographia in PD is known to occur in two forms: constant micrographia and progressive micrographia. In constant micrographia, the letter size is consistently small, while in progressive micrographia, letter size reduces progressively during the course of a sentence or a word (see Marjama-Lyons and Koller, 2007, for handwriting samples showing progressive micrographia in PD patients). In the simulation studies shown so far, striatal dopamine levels are assumed to be tonic. However, in reality, striatal dopamine is depleted gradually until it is replenished by a fresh dopamine burst from SNc. Therefore, one must consider the effect of a variable dopamine signal on handwriting. Kilpatrick, Rooney, Michael, and Wightman (2000) show how striatal dopamine activity habituates to bouts of rewarding stimulation given to median forebrain regions. (An excellent discussion of the computational significance of phasic changes in striatal dopamine is available in chapter 3 of Daw, 2003). Depletion of striatal dopamine is understandable since neurotransmitter stores deplete over time, and there are also regulatory mechanisms that control transmitter release. It may be expected that in PD conditions, with reduced numbers of SNc dopaminergic neurons, this depletion may occur over shorter durations. It will be interesting to see the effect of depletion of striatal dopamine over the time taken to write a sentence or a single word on handwriting output.

To this end we make the model described in section 4 to produce a sequence of strokes *llllll*. To produce this sequence, the inputs of the handwriting network are fired in a sequence with appropriate temporal spacing between them: the input corresponding to e is fired first, following which the l input is fired five times in a sequence. Handwriting output produced under normal conditions (DA $= 50$, $\varepsilon = 0$) is shown in Figure 18a. When dopamine is linearly decreased from 50 to 5 over the entire word, there is a gradual reduction in letter size resembling progressive micrographia (see Figure 18b). When ε is set to 0.6 while dopamine is linearly decreased from 50 to 5, there is no progressive reduction in letter size, but the letter contour is more "kinky" (see Figure 18c).

6 Discussion

We present a model of PD handwriting in which the model is coupled with a BG model that emphasizes the role of the indirect pathway under PD conditions. PD pathologies are simulated by varying striatal dopamine (DA) and the GPe connectivity parameter (ε). Our model is similar in overall organization to the PD handwriting model of Contreras-Vidal and Stelmach (1995), though the components vastly differ. Further, we intend to relate the PD-related rhythm changes in STN-GPe to handwriting distortions. The oscillatory activity of the STN-GPe system has been linked to PD tremor in earlier studies. Synchronized high-frequency oscillations are found in STN

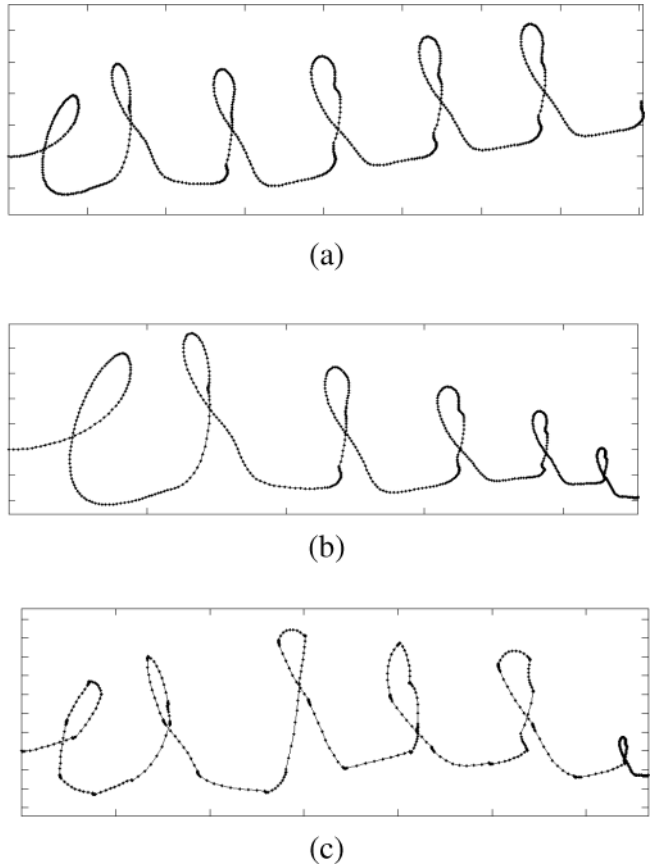

Figure 18: The word *elllll*. (a) Normal: DA = 50 constant and $\varepsilon = 0.0$. (b) Progressive micrographia: DA = decreases linearly from 50 to 5 with time and $\varepsilon = 0.0$. (c) Uneven letter size and kinky contour: DA decreased linearly from 50 to 5 with time and ε kept constant at 0.6.

neurons of PD patients with tremor; dopaminergic medication reduced the synchrony of STN neurons (Levy et al., 2002).

A coarse mapping of our handwriting network architecture onto neuroanatomy can be suggested. The input layer represents the dorsolateral prefrontal cortex (DLPFC), whose role in motor planning is well recognized (Fuster, 1997). The oscillatory layer represents the supplementary motor area (SMA) since data from primate motor research suggest that motor preparation is executed jointly by SMA and BG (Tanji, 1994). Modulation of the output of handwriting network by BG model output is analogous to the action gating function of basal ganglia (Houk, Davis, & Beiser, 1995). It

is thought that the striatum provides intermittent, focused inhibition within output structures that otherwise maintain inhibitory control over motor and cognitive systems throughout the brain (Harner, 1997). The output layer of handwriting network may be considered as a "lumped" representation including the primary motor area (M1) and all the motor structures lower in the motor hierarchy. (For a more detailed justification of neuromotor interpretation of the network architecture refer to Gangadhar et al., 2007).

Since our main objective is to represent PD pathologies as manifest in handwriting, we present a model of BG in which the indirect pathway is emphasized. Two changes mark PD conditions in the BG model: reduced dopamine represented by the parameter DA and altered dynamics of STN-GPe controlled by the parameter ε. Although these two parameters are varied independently in the handwriting results of Figure 15, synchronized oscillations of STN-GPe seem to be the result of reduced dopamine conditions in PD. Therefore, strictly speaking, in order to simulate PD conditions in the model, the two parameters have to be varied (reducing DA and increasing ε) together.

Although the simulations presented in this letter suggest that synchronized oscillations of STN-GPe system may be related to PD handwriting distortions, we have not explained, for reasons of space, the purpose of complex activity of STN-GPe in normal conditions. Complex STN-GPe dynamics seem to be necessary for the exploration of output space (Sridharan et al., 2006) as a part of the reinforcement learning that BG nuclei are thought to subserve (Doya, 2000). This larger picture of the role of STN-GPe in BG dynamics is developed elsewhere (Joseph, Garipelli, & Chakravarthy, 2007). Several instances have been discovered in physiology when the chaotic activity of a system is essential for its normal function (Goldberger, Rigney, & West, 1990). It appears that we have a similar situation in the STN-GPe system: complex activity corresponds to normal function and loss of complexity to disease.

Handwriting produced under PD "pathological" regimes of these parameters exhibits classic PD handwriting distortions as follows:

- *Micrographia*. Reduction of dopamine levels in the model shows reduced handwriting size analogous to micrographia. Experimental studies on PD patients show evidence for significantly smaller strokes, decreased mean acceleration, and diminished peak velocity in PD patients than normal controls (van Gemmert et al., 2003).
- *Progressive micrographia*. When striatal dopamine levels are reduced linearly, a progressive reduction in stroke size is observed in the model. However, such a monotonic size reduction did not occur when $\varepsilon = 0.6$ (the STN-GPe system operates in a "clustering" regime). The model suggests that whether micrographia is of the progressive or constant type probably depends not only on rapid dopamine depletion but also on the dynamics of STN-GPe. Confirmation of this

prediction can come from detailed experimental studies that link the type of micrographia with the state of BG pathology.

- *Bradykinesia*. Since, in the model, stroke output essentially rides over a cycle of the rhythm generated by the oscillatory layer, the property of isochrony emerges naturally in the model. The model generates all the strokes in more or less the same time, which does not vary in dopamine-depleted conditions since oscillation frequency does not change. Since a smaller letter is written over the same duration, the overall movement is slower. Experimental studies reveal that average stroke duration of the patients with PD is no longer than the average stroke duration of normal controls (van Gemmert et al., 2003).
- *Tremor in handwriting*. Tremor in handwriting can be observed when the STN-GPe system operates in a regular regime. Low-frequency synchronous burst activity in the STN–GPe loop may propagate down the motor system, contributing to jagged handwriting.

An essential idea that emerges out of this model is that rhythm-related distortions in PD motor performance are closely related to the dynamics of STN-GPe. This is not surprising since the STN-GPe system has been described as the "pacemaker of basal ganglia" (Bevan, Magill, Terman, Bolam, & Wilson, 2002). Tass (2003) argues that the synchronized and periodic firing of neurons in the thalamus and the basal ganglia causes Parkinsonian resting tremor, with these neurons influencing the premotor areas and the motor cortex. Therefore, desynchronization of these synchronized firing patterns has been suggested as a strategy for deep brain stimulation (DBS) procedures (Tass, 2003). In our model, the STN-GPe system plays the role of these neurons with activity patterns of the STN-GPe system influencing handwriting features. The model makes a precise prediction in this matter. When the STN-GPe system operates in synchronized cluster mode, it is observed that handwriting shows unusual velocity fluctuations and a "kinky" contour. Very often the pen tip (in simulation) slows down as it approaches a "kink," makes a sharp change in direction, and accelerates again. The precise instant at which such a kink occurs coincides with a synchronized burst in the STN-GPe neurons in the model, as was observed in animated simulations (see Figure 19b). This would be an interesting prediction to confirm or reject with the help of an experiment. However, the experiment for verifying this prediction may not be trivial. One source of such data is a PD patient undergoing DBS surgery. In these surgeries, exploratory probing has to be done to locate BG nuclei precisely. Encouraging the patient to perform simple handwriting tasks while the activity of STN-GPe system is monitored is an option. However, such a task places too high a demand on a patient who is already facing a traumatic challenge. Simpler experimental techniques that unravel the link between STN-GPe activity and motor function, should they exist, are preferable.

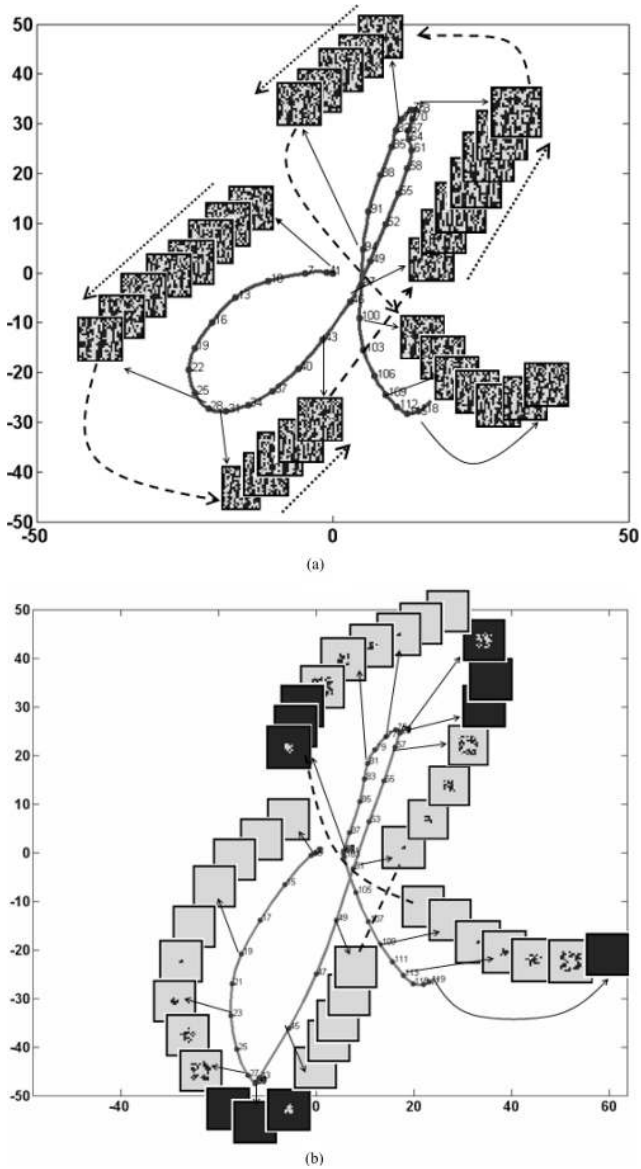

Figure 19: Dynamics of the STN-GPe network are correlated with episodes in handwritten segments. (a) Normal handwriting. The stroke has a smooth profile and the dynamics of the STN network has complex activity. (b) PD handwriting. The stroke is kinky in nature, and the dynamics of the STN network is in the clustered regime (correlated activity). Also it may be noteworthy that abrupt changes in pen movement direction correspond to transient periods of bursting activity in the STN-GPe system.

Acknowledgments

We thank Arun Kumar and E.S. Krishnamoorthy for providing the handwriting samples in Figure 1b of a PD patient.

References

Bergman, H., Whichman, T., Karmon, B., & DeLong, M. R. (1994). The primate subthalamic nucleus. II. Neural activity in MPTP model of Parkinsonism. *J. Neurophysiol.*, *72*, 507–520.

Beuter, A., & Vasilakos, K. (1995). Is Parkinson's disease a dynamical disease? *Chaos*, *5*, 35–42.

Bevan, M., D., Magill, P. J., Terman, D., Bolam, J. P., & Wilson, C. J. (2002). Move to the rhythm: Oscillations in the subthalamic nucleus-external globus pallidus network. *Trends in Neurosciences*, *25*, 525–531.

Borrett, D. S., Yeap, T. H., & Kwan, H. C. (1993). Neural networks and Parkinson's disease. *Canadian Journal of Neurological Sciences*, *20*, 107–113.

Bressloff, P. C., Coombes, S., & Souza, B. (2002). Dynamics of a ring of pulse-coupled oscillators: Group theoretic approach. *Physical Review Letters*, *66*, 2791–2794.

Brown, P., Olivero, A., Mazzone, P., Insola, A., Tonali, P., & Lazzaro, V. D. (2001). Dopamine dependency of oscillations in between subthalamic nucleus and pallidum in Parkinson's disease. *J. Neurosci.*, *21*, 1033–1038.

Buhusi, C. V., & Meck, W. H. (2005). What makes us tick? Functional and neural mechanisms of interval timing. *Nat. Rev. Neurosci.*, *6*, 755–756

Bullock, D., & Grossberg, S. (1988). The VITE model: A neural command circuit for generating arm and articulator trajectories. In A. Kelso & M. M. Shlesinger (Eds.), *Dynamic patterns in complex systems*. Singapore: World Scientific.

Clark, D., Boutros, N., & Mendez, M. (2005). *The brain and behavior*. Cambridge: Cambridge University Press.

Cobbah, W. G. K., & Fairhurst, M. C. (2000). Computer analysis of handwriting dynamics during dopamimetic tests in Parkinson's disease. In *Proceedings of the 26th EUROMICRO Conference* (pp. 2414–2418). Washington, DC: IEEE Computer Society.

Contreras-Vidal, J. L., & Stelmach, G. E. (1995). A neural model of basal ganglia-thalamocortical relations in normal and parkinsonian movement. *Biological Cybernetics*, *73*, 467–476.

Contreras-Vidal, J. L., & Stelmach, G. E. (1996). Effects of Parkinsonism on motor control. *Life Sciences*, *58*, 165–176.

Daw, N. (2003). *Reinforcement learning models of the dopamine system and their behavioral implications*. Unpublished doctoral dissertation, Carnegie Mellon University.

Doya, K. (2000). Complementary roles of basal ganglia and cerebellum in learning and motor control. *Current Opinion in Neurobiology*, *10*(6), 732–739.

Edwards, R., Beuter, A., & Glass, L. (1999). Parkinsonian tremor and simplification in network dynamics. *Bulletin of Mathematical Biology*, *61*, 157–177.

Fuster, J. (1997). *The prefrontal cortex: Anatomy, physiology, and neuropsychology of the frontal lobes*. New York: Raven.

Gallucci, R. M., Phillips, J. G., Bradshaw, J. L., Vaddadi, K. S., & Pantelis, C. (1997). Kinematic analysis of handwriting movements in schizophrenic patients. *Biol. Psychiatry*, *41*, 830–833.

Gangadhar, G., Joseph, D., & Chakravarthy, V. S. (2007). An oscillatory neuromotor model of handwriting generation. *International Journal of Document Analysis and Recognition*, *10*, 69–84.

Gillies, A. D., Willshaw, D., & Li, Z. (2002). Subthalamic-pallidal interactions are critical in determining normal and abnormal functioning of the basal ganglia. *Proc. R. Soc. Lond. B.*, *269*, 545–551.

Goldberger, A. L., Rigney, D. R., & West, B. J. (1990). Chaos and fractals in human physiology. *Scientific American*, *262*, 42–49.

Harner, A. M. (1997). *An introduction to basal ganglia function*. Boston: Boston University.

Haykin, S. (1998). *Neural networks: A comprehensive foundation*. Upper Saddle River, NJ: Prentice Hall.

Hollerbach, J. M. (1981). An oscillation theory of handwriting. *Biological Cybernetics*, *39*, 139–156.

Houk, J. C., Davis, J. L., & Beiser, D. G. (1995). *Models of information processing in the basal ganglia*. Cambridge, MA: MIT Press.

Hurtado, J. M., Gray, C. M., Tamas, L. B., & Sigvardt, K. A. (1999). Dynamics of tremor-related oscillations in the human globus pallidus: A single case study. *Proc. Natl. Acad. Sci. USA, 96*, 1674–1679.

Joseph, D., Garipelli, G., & Chakravarthy, V. S., (2007). *ACE (Actor-Critic-Explorer) paradigm for reinforcement learning in basal ganglia: Highlighting the role of subthalamic and pallidal nuclei*. Manuscript submitted for publication.

Kalveram, K. T. (1996). A neural oscillator model learning given trajectories, or how an allo-imitation algorithm can be implemented into a motor controller. In J. Piek (Ed.), *Motor behavior and human skill*. Champaign, IL: Human Kinetics.

Kilpatrick, M. R., Rooney, M. B., Michael, D. J., & Wightman, R. M. (2000). Extracellular dopamine dynamics in rat caudate-putamen during experimenter-delivered and intracranial self-stimulation. *Neuroscience*, *96*, 697–706.

Kuenstler, U., Juhnhold, U., Knapp, W. H., & Gertz, H. J. (1999). Positive correlation between reduction of handwriting area and D2 dopamine receptor occupancy during treatment with neuroleptic drugs. *Psychiatry Research: Neuroimaging*, *90*, 31–39.

Levy, R., Ashby, P., Hutchison, W. D., Lang, A. E., Lozano A. M., & Dostrovsky J. O. (2002). Dependence of subthalamic nucleus oscillations on movement and dopamine in Parkinson's disease. *Brain*, *125*, 1196–1209(14).

Marjama-Lyons, J. M, & Koller, W. C. (2007). Parkinson's disease: Update in diagnosis and symptom management. *Geriatrics*, *56*, 24–35.

Mavrogiorgou, P., Mergl, R., Tigges, P., Husseini, J. E., Schröter, A., Juckel, G., et al. (2001). Kinematic analysis of handwriting movements in patients with obsessive-compulsive disorder. *J. Neurol. Neurosurg. Psychiatry*, *70*, 605–612.

Mitchel, I. J., Brotchie, J. M., & Crossman, A. R. (1991). Modeling the fuctional organization of the basal ganglia: A parallel distributed processing approach. *Movement Disorders*, *6*, 189–204.

Montague, P. R., Dayan, P., Person, C., & Sejnowski, T. J. (1995). Bee foraging in uncertain environments using predictive Hebbian learning. *Nature*, *377*, 725–728.

Phillips, J. G., Bradshaw, J. L., Chiu, E., & Bradshaw, J. A. (1994). Characteristics of handwriting of patients with Huntington's disease. *Movement Disorders*, *9*, 521–530.

Phillips, J. G., Stelmach, G. E., & Teasdale, N. (1991). What can indices of handwriting quality tell us about Parkinsonian handwriting? *Human Movement Science*, *10*, 301–314.

Plamondon, R. (1989). An evaluation of motor models of handwriting. *IEEE Transactions on Systems, Man and Cybernetics*, *9*, 1060–1072.

Schomaker, L. R. B. (1991). *Simulation and recognition of handwriting movements: A vertical approach to modeling human motor behavior*. Unpublished doctoral dissertation, Nijmegen University.

Schultz, W. (1998). Predictive reward signal of dopamine neurons. *J. Neurophysiol.*, *80*, 1–27.

Sridharan, D., Prashanth, P. S., & Chakravarthy, V. S. (2006). The role of the basal ganglia in exploration in a neural model based on reinforcement learning. *Int. J. Neural Syst*., *16*, 111–124.

Suri, R. E., Albani, C., & Glattfelder, A. H. (1997). A dynamic model of motor basal ganglia functions. *Biological Cybernetics*, *76*, 451–458.

Tanji, J. (1994). The supplementary motor area in the cerebral cortex. *Neurosci. Res*., *19*, 251–268.

Tass, P. A. (2003). A model of desynchronizing deep brain stimulation with a demand-controlled coordinated reset of neural subpopulations. *Biological Cybernetics*, *89*, 81–88.

Terman, D., Rubin, J. E., Yew, A. C., & Wilson, C. J. (2002). Activity patterns in a model for the subthalamopallidal network of the basal ganglia. *J. Neurosci*., *22*, 2963–2976.

Teulings, H. L., & Stelmach, G. E. (1991). Control of stroke size, peak acceleration, and stroke duration in Parkinsonian handwriting. *Human Movement Science*, *10*, 315–334.

Teulings, H. L., Vidal, C. J. L., Stelmach, G. E., & Adler, C. H. (2002). Handwriting size adaptation under distorted visual feedback in Parkinson's disease patients, elderly controls and young controls. *Journal of Neurology, Neurosurgery, and Psychiatry*, *72*, 315–324.

Van Gemmert, A. W. A., Adler, C. H., & Stelmach, G. E. (2003). Parkinson's disease patients undershoot target size in handwriting and similar tasks. *Journal of Neurology, Neurosurgery, and Psychiatry*, *74*, 1502–1508.

Van Gemmert, A. W. A., Teulings, H. L., Contreras-Vidal, J. L., & Stelmach, G. E. (1999). Parkinson's disease and the control of size and speed in handwriting. *Neuropsychologica*, *37*, 685–694.

Received March 29, 2007; accepted December 28, 2007.